Appl. Math. Mech. -Engl. Ed., **33**(5), 605–620 (2012)
DOI 10.1007/s10483-012-1574-7

Applied Mathematics and Mechanics (English Edition)

Influence of magnetic field and thermal radiation by natural convection past vertical cone subjected to variable surface heat flux*

G. PALANI[1], K. Y. KIM[2]

(1. Department of Mathematics, Dr. Ambedkar Govt. Arts College,
Chennai 600039, Tamil Nadu, India;
2. Department of Mechanical Engineering, Inha University,
Incheon 402751, Republic of Korea)

Abstract A numerical study is performed to examine the heat transfer characteristics of natural convection past a vertical cone under the combined effects of magnetic field and thermal radiation. The surface of the cone is subjected to a variable surface heat flux. The fluid considered is a gray, absorbing-emitting radiation but a non-scattering medium. With approximate transformations, the boundary layer equations governing the flow are reduced to non-dimensional equations valid in the free convection regime. The dimensionless governing equations are solved by an implicit finite difference method of Crank-Nicolson type which is fast convergent, accurate, and unconditionally stable. Numerical results are obtained and presented for velocity, temperature, local and average wall shear stress, and local and average Nusselt number in air and water. The present results are compared with the previous published work and are found to be in excellent agreement.

Key words apex, magnetohydrodynamics, radiation, finite difference, skin friction, vertical cone

Chinese Library Classification O357
2010 Mathematics Subject Classification 76W05

1 Introduction

Free convection flow and heat transfer problems are of important considerations in the thermal design of a variety of industrial equipment, nuclear reactors, and geophysical fluid dynamics. The transient natural convection flows over a vertical bodies has a wide range of applications in engineering and technology. These kinds of enhances heat transfer around various kind of electrical and electronic devices, nuclear reactors play an important role in manufacturing process such as hot extrusion, metal forming, crystal growing, and heat transfer effects. In particular, the study of enhanced heat transfer is very useful in cone surfaces. When a heated surface is in contact with the fluid, the result of temperature difference causes buoyancy force, which induces the natural convection. Heat flux applications are widely used in industries, engineering, and science fields. Heal flux sensors can be used in industrial measurement and control systems. Examples of few applications are detection fouling (boiler fouling sensor), monitoring of furnaces (blast furnace monitoring/general furnace monitoring), and flare monitoring.

* Received Oct. 29, 2011 / Revised Jan. 4, 2012
Corresponding author G. PALANI, Ph. D., E-mail: gpalani32@yahoo.co.in

Numerous authors have investigated laminar natural convection flow problem for two-dimensional axisymmetric flows. Merk and Prins[1–2] developed the general relation for similar solutions on isothermal axisymmetric forms, and they showed that the vertical cone has such a solution in steady state. Alamgir[3] investigated the overall heat transfer in laminar natural convection from a vertical cone using the integral method. Pop and Takhar[4] studied the compressibility effects in laminar free convection from a vertical cone. Pop et al.[5] analyzed the steady laminar mixed convection boundary layer flow over a vertical isothermal cone for fluids of any values of Pr for both the cases of buoyancy assisting and buoyancy opposing flow conditions. The resulting non-similarity boundary layer equations are solved numerically using the Keller-box scheme. Takhar et al.[6] discussed the effects of thermo physical quantities on the free convection flow of gases over an isothermal vertical cone in steady-state flow, in which thermal conductivity, dynamic viscosity, and specific heat at constant pressure were assumed to have a power law variation with absolute temperature. Recently, theoretical studies on laminar free convection flow over an axisymmetric body have received wide attention especially in case of uniform and non-uniform surface heat flux distributions. Similarity solutions for the laminar free convection from a right circular cone with prescribed uniform heat flux conditions were reported by Lin[7]. Na and Chiou[8] investigated the laminar natural convection flow over a frustum of cone without transverse curvature effects. Gorla et al.[9] presented a numerical solution for laminar free convection of power-law fluids past a vertical frustum of a cone without transverse curvature effect (i.e., large cone angles when the boundary layer thickness is small compared with the local radius of the cone). Kumari and Pop[10] studied free convection from vertical rotating cone with uniform wall heat flux. Hossain et al.[11] studied the non-similarity solution for the problem of laminar natural convection flow and heat transfer from a vertical circular cone immersed in a thermally stratified medium with either a uniform surface temperature or a uniform heat flux. Using a finite difference method, a series solution method and asymptotic solution method, the solutions have been obtained for the non-similarity boundary layer equations. Recently, Bapuji et al.[12] studied transient laminar free convection from an incompressible viscous fluid past a vertical cone with non-uniform surface heat flux, varying as a power function of the distance from the apex of the cone. The non-dimensional governing equations are solved by using an implicit finite difference method.

Laminar free convection boundary-layer flow of an electrically conducting fluid in the presence of magnetic field has been investigated by many researchers because of its wide applications in industry and technological applications. The influence of a magnetic field on viscous incompressible flow of an electrically conducting fluid is of importance in many applications such as extrusion of plastics in the manufacture of rayon and nylon, purification of crude oil, magnetic materials processing, glass manufacturing control processes, and the paper industry in different geophysical cases. In many process industries, the cooling of threads or sheets of some polymer materials is of importance in the production line. Magneto convection plays an important role in various industrial applications including magnetic control of molten iron flow in the steel industry and liquid metal cooling in nuclear reactors.

Free convection heat transfer due to the simultaneous action of buoyancy and induced magnetic forces was investigated by Sparrow and Cess[13]. They observed that the free convection heat transfer to liquid metals may be significantly affected by the presence of a magnetic field. The interaction of thermal radiation with free convection heat transfer was studied by Cess[14]. Kumari and Nath[15] studied the development of the asymmetric flow of a viscous electrically conducting fluid in the forward stagnation point region of a two-dimensional body and over a stretching surface with an applied magnetic field when the external stream or the stretching surface was set into the impulsive motion from the rest. Takhar et al.[16] numerically investigated the unsteady mixed convection flow from a rotating vertical cone with a time dependent angular velocity under the influence of transverse magnetic field. Analysis of the unsteady laminar mixed convection about a spinning sphere with a magnetic field was recently given by

Ozturk[17]. Unsteady laminar heat and mass transfer from a rotating vertical cone with a magnetic field and heat generation or absorption effects was numerically investigated by Chamkha and Al-Mudhaf[18]. Laminar free convection boundary layer flow in the presence of a transverse magnetic field over a heated-down pointing cone spinning with constant angular velocity about the symmetry axis was studied by Mehmet[19] using similarity variables.

Radiative flows are encountered in countless industrial and environmental processes, e.g., heating and cooling chambers, fossil fuel combustion and energy processes, evaporation from large open water reservoirs, astrophysical flows, and solar power technology. Soundalgekar and Takhar[20] considered the radiative free convective flow of an optically thin gray-gas past a semi-infinite vertical plate. Radiation effects on mixed convection along an isothermal vertical plate were studied by Hossain and Takhar[21]. Raptis and Perdikis[22] studied the effects of thermal radiation and free convection flow past a moving vertical plate. Muthucumaraswamy and Ganesan[23] studied radiation effects on flow past an impulsively started infinite vertical plate with variable temperatures using the Laplace transform technique. Moreover, the magnetohydrodynamics (MHD) flow past a plate by the presence of radiation was studied by Raptis and Massalas[24]. The analytical solutions for the mean temperature, velocity and the magnetic field were arrived and the effects of radiation on temperature are discussed. The radiation effects on mixed convection over an isothermal cone in porous media with Rosseland diffusion approximation was investigated numerically by Yih[25].

The combined effects of thermal radiation flux, thermal conductivity, Reynolds number, and non-Darcian (Forcheimmer drag and Brinkman boundary resistance) body forces on a steady laminar boundary layer flow along a vertical surface in an idealized geological porous medium were investigated by Takhar et al.[26]. The effects of radiation on free convection flow and mass transfer past a vertical isothermal cone surface with chemical reaction in the presence of magnetic field were investigated by Ahmed[27] using similarity variables. The effects of thermal radiation and porous drag forces on the natural convection heat and mass transfer of a viscous, incompressible, gray, absorbing emitting fluid flowing past an impulsively started moving vertical plate adjacent to a non-Darcian porous regime were studied by Beg et al.[28]. The effect of radiation on MHD unsteady free-convection flow past a semi-infinite vertical porous plate in the presence of transversal uniform magnetic field was studied by Abd El-Naby et al.[29]. However, the influence of magnetic field and thermal radiation by natural convection past a vertical cone subjected to a variable surface heat flux has not received the attention of any researcher. The object of the present investigation is to study the combined effects of magnetic field and thermal radiation on the free convection flow past a semi-infinite vertical cone subjected to a variable surface heat flux, when the fluid is incompressible, viscous, and electrically conducting. The fluid considered is a gray, radiation, absorbing, emitting but non-scattering medium, and the Rosseland approximation is used to describe the radiative heat transfer in the energy equation. The set of non-dimensional governing equations are solved by the finite difference method.

2 Basic equations and mathematical analysis

An axisymmetric transient laminar free convection of a viscous, incompressible, and electrical conducting fluid of an uniform ambient temperature T'_∞ past a vertical cone with variable surface heat flux along with thermal radiation is considered. The uniform transverse magnetic field normal to the cone is applied. The radiative heat flux in the x direction is considered negligible in comparison with that in y direction. The fluid considered is a gray, absorbing-emitting radiation but a non-scattering medium. Initially, assumed that the cone surface and the surrounding fluid that is at rest. Then, at time $t' > 0$, it is assumed that heat is supplied from cone surface to the fluid at the rate $q_{\mathrm{w}}(x) = x^n$, and it is maintained at this value with n being a constant. The coordinate system is chosen (see Fig. 1) such that x measures the distance

along the surface of the cone from the apex ($x = 0$), and y measures the distance normally outward. Here, ϕ is the semi vertical angle of the cone, and r is the local radius of the cone. All the fluid properties are assumed to be constant except the influence of the density variation with temperature is considered only in the body force term, and it plays a predominant role in free convection.

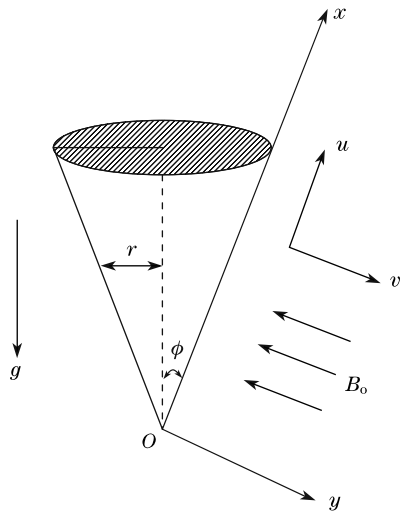

Fig. 1 Flow model and coordinate system

Magnetic field equations usually are the electromagnetic and hydromagnetic equations, but interaction between the motion and the magnetic field are considered. In most problems involving conductor Maxwell's displacement currents are neglected, so that electric currents are regarded as flowing in closed circuits. Assuming that the velocity of flow is too small compared with the velocity of light, i.e., the relativistic effects are ignored, the system of Maxwell's equation can be written in the following form[29–30]:

$$\nabla \times \overline{B} = \mu \bar{J}, \quad \nabla \cdot \bar{J} = 0,$$

$$\nabla \times \overline{E} = -\frac{\partial \overline{B}}{\partial t}, \quad \nabla \cdot \overline{B} = 0.$$

Ohm's law can be written in the form

$$\bar{J} = \sigma(\overline{E} + \overline{u} \times \overline{B}), \tag{1}$$

where $\overline{u}$ is the velocity vector, $\overline{E}$ is the electric field intensity, $\overline{B}$ is the magnetic induction intensity, μ is the magnetic field permeability, $\bar{J}$ is the electric current density, and σ is the electrical conductivity.

In the equation of motion, the body force $\bar{J} \times \overline{B}$ per unit volume is added. This body force represents the coupling between the magnetic field and the fluid motion which is called Lorentz force.

The induced magnetic field due to the motion of the electrically conducting fluid is negligible. This assumption is valid for a small Reynolds number. This is rather important for some practical engineering problems, where the conductivity is not large, in the absence of an external applied field with negligible effects of polarization of the ionized gas. It has been taken $\overline{E} = 0$ (i.e., in the absence of convection outside the boundary layer, $\overline{B} = \overline{B}_0$ and $\nabla \times \overline{B} = \mu \bar{J}$. Thus, $\overline{E} = 0$).

The Lorentz force becomes $\bar{J} \times \overline{B} = \sigma\left(\overline{u} \times \overline{B}\right) \times \overline{B}$. In what follows, the induced magnetic field will be neglected. This is justified, if the magnetic Reynolds number is small. Hence, to get a better approximation, the Lorentz force can be replaced by $\sigma\left(\overline{u} \times \overline{B}_0\right) \times \overline{B}_0 = -\sigma B_0^2 \overline{u}$.

The induced magnetic field due to the motion of the electrically conducting fluid is negligible. This assumption is valid for a small Reynolds number. Neglecting the viscous, pressure gradient, and magnetic dissipation, and taking account of the Boussinesq approximation, we obtain the governing boundary layer equations as follows:

$$\frac{\partial(ru)}{\partial x} + \frac{\partial(rv)}{\partial y} = 0, \tag{2}$$

$$\frac{\partial u}{\partial t'} + u\frac{\partial u}{\partial x} + v\frac{\partial u}{\partial y} = g\beta(T' - T'_\infty)\cos\phi + \nu\frac{\partial^2 u}{\partial y^2} - \frac{\sigma B_0^2}{\rho}u, \tag{3}$$

$$\rho c_p\Big(\frac{\partial T'}{\partial t'} + u\frac{\partial T'}{\partial x} + v\frac{\partial T'}{\partial y}\Big) = k\frac{\partial^2 T'}{\partial y^2} - \frac{\partial q_r}{\partial y}, \tag{4}$$

where the Rosseland approximation[31] is used, which leads to

$$q_r = \frac{-4\sigma^*}{3k^*}\frac{\partial T'^4}{\partial y}. \tag{5}$$

The initial and boundary conditions are
(i) $t' \leqslant 0$ (for all x and y)

$$u = 0, \quad v = 0, \quad T' = T'_\infty, \tag{6a}$$

(ii) $t' > 0$

$$\begin{cases} u = 0, \quad v = 0, \quad \dfrac{\partial T'}{\partial y} = -\dfrac{q_{\mathrm{w}}(x)}{k}, \quad y = 0, \\ u = 0, \quad T' = T'_\infty, \quad x = 0, \\ u \to 0, \quad T' \to T'_\infty, \quad y \to \infty. \end{cases} \tag{6b}$$

We assumed that the temperature differences within the flow are sufficiently small such that T'^4 may be expressed as a linear function of the temperature. This is accomplished by expanding T'^4 in Taylor series about T'_∞ and neglecting higher-order terms. Thus,

$$T'^4 \cong 4T'^3_\infty T' - 3T'^4_\infty. \tag{7}$$

Using (5) and (7) in (4), we get

$$\rho c_p\Big(\frac{\partial T'}{\partial t'} + u\frac{\partial T'}{\partial x} + v\frac{\partial T'}{\partial y}\Big) = k\frac{\partial^2 T'}{\partial y^2} + \frac{16\sigma^* T'^3_\infty}{3k^*}\frac{\partial^2 T'}{\partial y^2}, \tag{8}$$

where u and v are the velocity components along x and y directions respectively, T' is the temperature of the fluid in the boundary layer, T'_∞ is the temperature far away from the plate, t' is the time, g is the acceleration due to gravity, r is the local radius of the cone, k is the thermal conductivity of the fluid, β is the volumetric coefficient of thermal expansion, ρ is the density, c_p is the specific heat, ϕ is the semi-vertical angle of the cone, ν is the kinematic

viscosity, B_0^2 is the magnetic field induction, k^* is the absorption coefficient, σ is electrical conductivity, σ^* is Stefan Boltzmann constant, and μ is the coefficient of viscosity.

The physical quantities of interest are the local skin friction τ_x and the local Nusselt number Nu_x, which are given respectively by

$$\tau_x = \mu\Big(\frac{\partial u}{\partial y}\Big)_{y=0}, \quad Nu_x = \frac{x}{T'_{\rm w} - T'_\infty}\Big(-\frac{\partial T'}{\partial y}\Big)_{y=0}. \tag{9}$$

Also, the average skin friction $\overline{\tau}_{\rm L}$ and the average heat transfer coefficient $\overline{h}$ over the cone surface are given by

$$\overline{\tau}_{\rm L} = \frac{2\mu}{L^2}\int_0^L x\Big(\frac{\partial u}{\partial y}\Big)_{y=0}{\rm d}x, \quad \overline{h} = \frac{2k}{L^2}\int_0^L \frac{x}{T'_{\rm w} - T'_\infty}\Big(-\frac{\partial T'}{\partial y}\Big)_{y=0}{\rm d}x. \tag{10}$$

Thus, the average Nusselt number is given by

$$\overline{Nu}_{\rm L} = \frac{L\overline{h}}{k} = \frac{2}{L}\int_0^L \frac{x}{T'_{\rm w} - T'_\infty}\Big(-\frac{\partial T'}{\partial y}\Big)_{y=0}{\rm d}x. \tag{11}$$

We introduce the following non-dimensional quantities:

$$\begin{cases} X = \dfrac{x}{L}, \quad Y = \dfrac{y}{L}Gr_{\rm L}^{1/5}, \quad U = \dfrac{uL}{\nu}Gr_{\rm L}^{-2/5}, \\[2ex] V = \dfrac{vL}{\nu}Gr_{\rm L}^{-1/5}, \quad t = \dfrac{\nu t'}{L^2}Gr_{\rm L}^{2/5}, \quad R = \dfrac{r}{L}, \\[2ex] T = \dfrac{T' - T'_\infty}{\frac{q_{\rm w}(L)L}{k}}Gr_{\rm L}^{1/5}, \quad Gr_{\rm L} = \dfrac{g\beta q_{\rm w}(L)L^4}{\nu^2 k}\cos\phi, \quad Pr = \dfrac{\mu c_p}{k}, \\[2ex] N = \dfrac{k^*k}{4\sigma^* T'^3_\infty}, \quad M = \dfrac{\sigma B_0^2 L^2}{\rho\nu}Gr_{\rm L}^{-2/5}, \end{cases} \tag{12}$$

where Pr is the Prandtl number of the fluid, M is the magnetic field parameter, N is the Rosseland or Stark conduction radiation parameter, $Gr_{\rm L}$ is the modified Grashof number, L is the reference length.

The boundary layer remains thin because it grows less quickly than the radius of the cone. The local radius to a point in the boundary layer can be replaced by the radius of the cone surface, i.e.,

$$x = r\sin\phi.$$

(2), (3), and (8) are reduced to the following dimensionless forms:

$$\frac{\partial U}{\partial X} + \frac{\partial V}{\partial Y} + \frac{U}{X} = 0, \tag{13}$$

$$\frac{\partial U}{\partial t} + U\frac{\partial U}{\partial X} + V\frac{\partial U}{\partial Y} = T + \frac{\partial^2 U}{\partial Y^2} - MU, \tag{14}$$

$$\frac{\partial T}{\partial t} + U\frac{\partial T}{\partial X} + V\frac{\partial T}{\partial Y} = \frac{1}{Pr}\frac{(3N+4)}{(3N)}\frac{\partial^2 T}{\partial Y^2}. \tag{15}$$

The corresponding initial and boundary conditions in a dimensionless form are as follows:
(i) $t \leqslant 0$ (for all X and Y)

$$U = 0, \quad V = 0, \quad T = 0, \tag{16a}$$

(ii) $t > 0$

$$\begin{cases} U = 0, \quad V = 0, \quad \dfrac{\partial T}{\partial Y} = -X^n, \quad Y = 0, \\ U = 0, \quad T = 0, \quad X = 0, \\ U \to 0, \quad T \to 0, \quad Y \to \infty. \end{cases} \tag{16b}$$

The local non-dimensional skin friction and the local Nusselt number are given by

$$\tau_X = Gr_{\mathrm{L}}^{3/5} \Big(\frac{\partial U}{\partial Y}\Big)_{Y=0}, \quad Nu_X = \frac{Gr_{\mathrm{L}}^{1/5}}{T_{Y=0}} X^{n+1}. \tag{17}$$

Also, the non-dimensional average skin friction and the average Nusselt number are given by

$$\overline{\tau} = 2Gr_{\mathrm{L}}^{3/5} \int_0^1 X \Big(\frac{\partial U}{\partial Y}\Big)_{Y=0} \mathrm{d}X, \quad \overline{Nu} = 2Gr_{\mathrm{L}}^{1/5} \int_0^1 \frac{X^{n+1}}{T_{Y=0}} \mathrm{d}X. \tag{18}$$

3 Numerical techniques

An implicit finite difference scheme of Crank-Nicolson type has been used to solve the governing non-dimensional equations (13)–(15) under the initial and boundary conditions (16). The method of solving the above finite difference equations using Crank-Nicolson type has been discussed by Bapuji et al.[12]. The region of integration is considered as a rectangle with sides $X_{\max}\,(=1)$ and $Y_{\max}\,(=18)$, where $Y_{\max}$ corresponds to $Y = \infty$, which lies very well outside the momentum and thermal boundary layers. The maximum of Y was chosen as 18 after some preliminary investigations so that the last two of the boundary conditions (16) are satisfied. To obtain an economical and reliable grid system for the computations, a grid independence is performed. After experimenting with few sets of mesh sizes, they have been fixed at the level $\triangle X = 0.01$, $\triangle Y = 0.02$, and the time step $\triangle t = 0.01$. In this case, spatial mesh sizes are reduced by 50% in one direction, then in both directions, and the results are compared. It is observed that, when mesh size is reduced by 50% in X-direction and Y-direction, the results differ in fourth decimal place. Hence, the above mentioned sizes have been considered as appropriate mesh sizes for calculation. Computations are carried out until the steady-state is reached. The steady-state solution is assumed to have been reached, when the absolute difference between the values of U, as well as temperature T at two consecutive time steps are less than 10^{-5} at all grid points.

The derivatives involved in (17) and (18) are evaluated using a five point approximation formula, and then the integrals are evaluated using Newton-Cotes closed integration formula.

4 Stability and convergence of finite difference scheme

The stability criterion of the finite difference scheme for constant mesh sizes are examined using von-Neumann technique as explained by Carnahan et al.[32]. The general terms of the Fourier expansion for U and T at a time arbitrarily called $t = 0$, are assumed to be of the form

$e^{i\alpha X}e^{i\beta Y}$ (here, $i=\sqrt{-1}$). At later time t, these terms become

$$\begin{cases} U = F(t)e^{i\alpha X}e^{i\beta Y}, \\ \\ T = G(t)e^{i\alpha X}e^{i\beta Y}. \end{cases} \tag{19}$$

Substitute (19) into the finite difference forms of (14) and (15), under the assumption that the coefficients U and T are constants over any one time step and denoting the values after one time step by F' and G'. After simplification, we get

$$\frac{(F'-F)}{\triangle t}+\frac{U}{2}\frac{(F'+F)(1-e^{-i\alpha\triangle X})}{\triangle X}+\frac{V}{2}\frac{(F'+F)i\sin(\beta\triangle Y)}{\triangle Y}$$

$$=\frac{(G'+G)}{2}+\frac{(F'+F)(\cos(\beta\triangle Y)-1)}{(\triangle Y)^2}-\frac{M}{2}(F'+F), \tag{20}$$

$$\frac{(G'-G)}{\triangle t}+\frac{U}{2}\frac{(G'+G)(1-e^{-i\alpha\triangle X})}{\triangle X}+\frac{V}{2}\frac{(G'+G)i\sin(\beta\triangle Y)}{\triangle Y}$$

$$=\frac{1}{Pr}\frac{3N+4}{3N}\frac{(G'+G)(\cos(\beta\triangle Y)-1)}{(\triangle Y)^2}. \tag{21}$$

Equations (20) and (21) can be rewritten as

$$(1+A)F'=(1-A)F+\frac{(G'+G)}{2}\triangle t, \tag{22}$$

$$(1+B)G'=(1-B)G, \tag{23}$$

where

$$A=\frac{U}{2}\frac{\triangle t}{\triangle X}(1-e^{-i\alpha\triangle X})+\frac{V}{2}\frac{\triangle t}{\triangle Y}i\sin(\beta\triangle Y)-(\cos(\beta\triangle Y)-1)\frac{\triangle t}{(\triangle Y)^2}+\frac{\triangle t}{2}M,$$

$$B=\frac{U}{2}\frac{\triangle t}{\triangle X}(1-e^{-i\alpha\triangle X})+\frac{V}{2}\frac{\triangle t}{\triangle Y}i\sin(\beta\triangle Y)-\frac{(\cos(\beta\triangle Y)-1)}{Pr}\frac{3N+4}{3N}\frac{\triangle t}{(\triangle Y)^2}.$$

After eliminating G' in (22) and using (23), we get

$$(1+A)F'=(1-A)F+\frac{G}{(1+B)}\triangle t. \tag{24}$$

Equations (24) and (23) can be written in a matrix form as follows:

$$\begin{pmatrix} F' \\ G' \end{pmatrix}=\begin{pmatrix} \frac{1-A}{1+A} & D_1 \\ 0 & \frac{1-B}{1+B} \end{pmatrix}\begin{pmatrix} F \\ G \end{pmatrix}, \tag{25}$$

where

$$D_1=\frac{\triangle t}{(1+A)(1+B)}.$$

Now, for the stability of the finite difference scheme, the modulus of each eigen value of the amplification matrix does not exceed unity. Since the matrix equation (25) is triangular,

the eigen values are its diagonal elements. The eigen values of the amplification matrix are $(1-A)/(1+A)$ and $(1-B)/(1+B)$. Assuming that, U is everywhere non-negative and V is everywhere non-positive, we get

$$A = 2a\sin^2\left(\frac{\alpha\triangle X}{2}\right) + 2c\sin^2\left(\frac{\beta\triangle Y}{2}\right) + \mathrm{i}(a\sin(\alpha\triangle X) - b\sin(\beta\triangle Y)) + \frac{M}{2}\triangle t,$$

where

$$a = \frac{U}{2}\frac{\triangle t}{\triangle X}, \quad b = \frac{|V|}{2}\frac{\triangle t}{\triangle Y}, \quad c = \frac{\triangle t}{(\triangle Y)^2}.$$

Since the real part of A is greater than or equal to zero,

$$\left|\frac{(1-A)}{(1+A)}\right| \leqslant 1.$$

Similarly,

$$\left|\frac{(1-B)}{(1+B)}\right| \leqslant 1.$$

Hence, the finite difference scheme is unconditionally stable. The local truncation error is $O(\triangle t^2 + \triangle Y^2 + \triangle X)$, and it tends to zero as $\triangle t$, $\triangle X$, and $\triangle Y$ tend to zero. Hence, the scheme is compatible. Stability and compatibility ensures the convergence.

5 Results and discussion

To ascertain the accuracy of our numerical results, the present results are compared with the previously published work in the literatures. The present numerical results for temperature profiles and local skin friction at $X = 1.0$ with $n = 0$, $N = 0$, $M = 0$ and for different values of Pr are compared with similarity solutions of Lin[7] which are shown in Table 1. It is observed that the results are in good agreement with each other.

Table 1 Comparison of steady state temperature and local skin friction at $X = 1.0$ with those of Lin[7] for uniform surface heat flux ($n = 0$, $N = 0$, and $M = 0$)

Pr	Temperature		Local skin-friction	
	Lin[7]	Present results	Lin[7]	Present results
0.72	1.786 5	1.788 40	1.224 0	1.227 05
1	1.632 7	1.634 54	1.079 7	1.082 62
2	1.363 3	1.364 77	0.829 3	0.831 55
4	1.150 8	1.151 69	0.637 3	0.638 78
6	1.046 4	1.047 08	0.546 2	0.547 36
8	0.979 6	0.980 01	0.489 5	0.490 40
10	0.931 4	0.931 58	0.449 4	0.450 21
100	0.567 5	0.562 89	0.184 0	0.183 11

The transient velocity and temperature profiles at $X = 1.0$ for different values of Prandtl number of the fluid are calculated numerically and are presented in the graphical form in Figs. 2–3. The velocity and temperature of the fluid increase with time until a temporal maximum is reached, and thereafter a moderate reduction is observed until the ultimate steady state is reached. The velocity gradient for air ($Pr = 0.71$) is always greater than water ($Pr = 7.0$). Physically, this is true because the increase in the Prandtl number is due to increase in the viscosity of the fluid, which makes the fluid thick and hence causes a decrease in the velocity of

the fluid. The effect of the Prandtl number is very important in the temperature field. A fall in temperature occurs due to an increasing value of the Prandtl number. This is in agreement with the physical fact that the thermal boundary layer thickness decreases with increasing Pr. Also, it is observed that the time taken to reach the steady state flow increases and thermal boundary layer thickness reduces with increasing Prandtl number of the fluid.

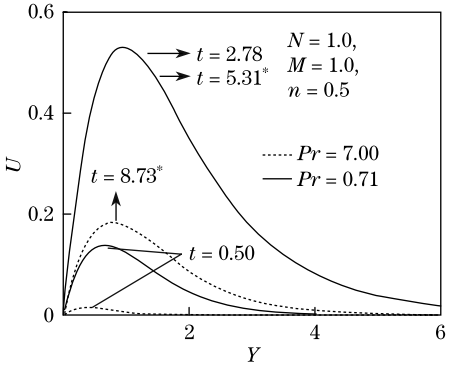

Fig. 2 Transient velocity profiles at $X = 1.0$ for different Pr (∗- steady state)

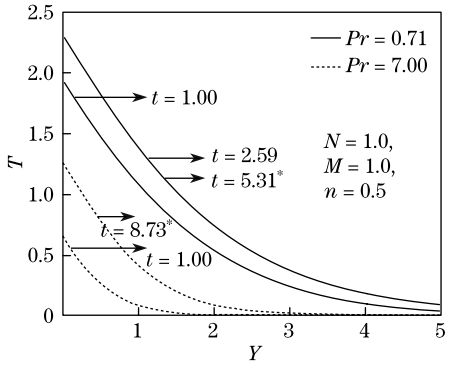

Fig. 3 Transient temperature profiles at $X = 1.0$ for different Pr (∗- steady state)

Figures 4 and 5 show that the velocity and temperature profiles at the leading edge of the cone, i.e., $X = 1.0$ for different values of exponent n. Impulsive driving forces are reduced along the surface of the cone near the apex for increasing value of n (i.e., the gradient of heat flux along the cone near the apex reduces with the increasing value of n). Due to this, the difference between temporal maximum values and steady state values reduces with the increasing value of n. No temporal maximum is observed for higher values of n.

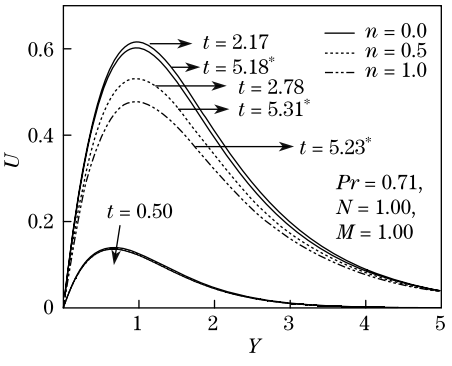

Fig. 4 Transient velocity profiles at $X = 1.0$ for different n (∗- steady state)

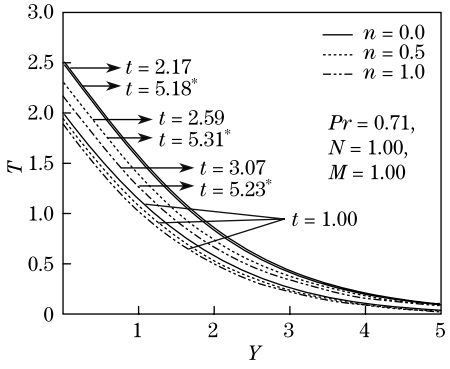

Fig. 5 Transient temperature profiles at $X = 1.0$ for different n (∗- steady state)

The transient velocity and temperature profiles for air at their temporal maximum and steady state against the coordinate Y at $X = 1.0$ for different radiation parameter N are shown in Figs. 6–7. It is seen that the temperature decreases as the radiation parameter N increases. This result qualitatively agrees with expectation since the effect of radiation is to decrease the rate of energy transport to the fluid, thereby decreasing the temperature of the fluid. It is observed that an increase in the radiation parameter leads to a fall in the velocity of air. Also, it is also noticed that the difference between the temporal maximum value and steady state value decreases with the increasing value of radiation parameter N. It is noticed

that the time required to reach the steady state flow decreases with the increasing value of radiation parameter N, this implies that the existence of radiation helps to achieve the steady state rapidly.

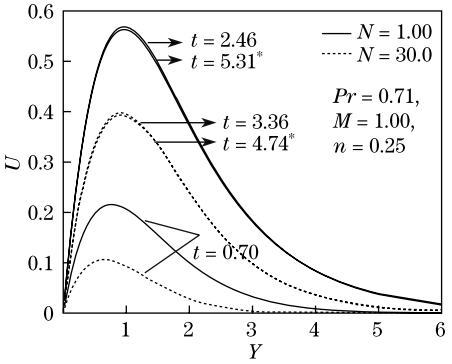

Fig. 6 Transient velocity profiles at $X = 1.0$ for different N ($*$- steady state)

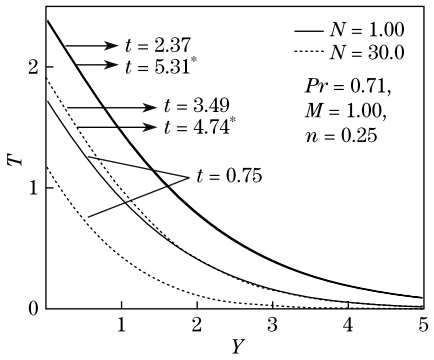

Fig. 7 Transient temperature profiles at $X = 1.0$ for different N ($*$- steady state)

Figures 8 and 9 represent the velocity and temperature distribution of air for different values of magnetic field parameter M. It is observed that the time taken to reach the steady state is more for higher values of magnetic field parameter in comparison with the lower values of magnetic field parameter. The difference between the temporal maximum and steady state decreases as M increases. No temporal maximum is observed for higher values of M. The effect of a transverse magnetic field on an electrically conducting fluid give rise to a resistive type force called Lorentz force. This force has tendency to slow down the motion of the fluid and to increases its temperature. The steady state velocity and temperature profile for different values of M at $X = 0.25$, 0.5, and 1.0 are shown in Fig. 10 and Fig. 11, respectively. The temperature and velocity increases along the surface of the cone. It is notice that the effect of magnetic field is greater at the leading edge, i.e., at $X = 1.0$.

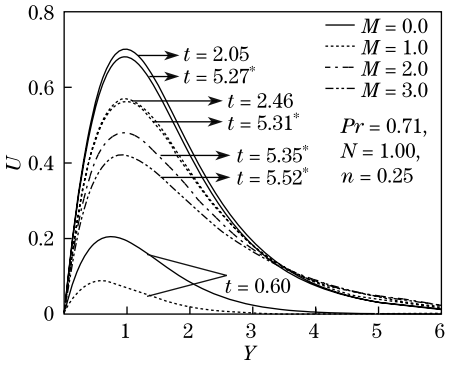

Fig. 8 Transient velocity profiles at $X = 1.0$ for different M ($*$- steady state)

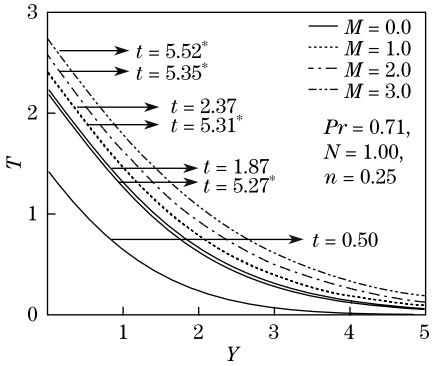

Fig. 9 Transient temperature profiles at $X = 1.0$ for different M ($*$- steady state)

The study of the effects of the parameters on the local as well as average shearing stress and the rate of heat transfer is important in the heat transfer problems. The steady state values of local skin friction and Nusselt number for different values of Prandtl number (Pr) and exponent n are calculated numerically from (17) and are depicted graphically in Fig. 12 and Fig. 13, respectively. The local skin friction decreases with the increasing value of n and the

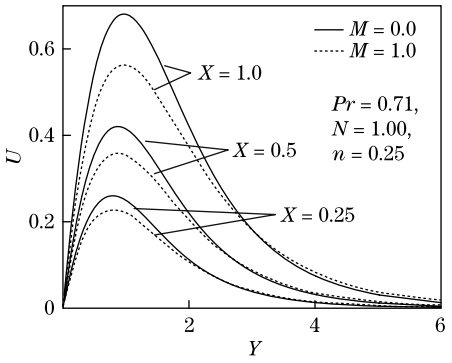

Fig. 10 Steady state velocity profiles for different M at $X = 0.25$, 0.5, and 1.0

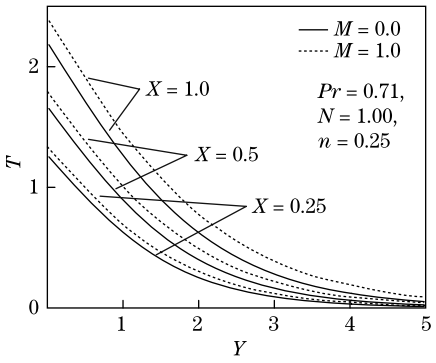

Fig. 11 Steady state temperature profiles for different M at $X = 0.25$, 0.5, and 1.0

effect of n over the local skin friction is more near the apex ($X = 0.0$) of the cone and reduces gradually with increasing the distance along the surface of the cone from the apex. The local Nusselt number reduces with the increasing value of exponent n near the apex of the cone, but the trend is slowly changed and reversed at distance increases along the surface from the cone. It is observed that the local skin friction decreases with the increasing Prandtl number of the fluid. The rate of heat transfer is stronger on Pr than on the other parameters, since a lower Pr gives thicker temperature profiles. Larger values of Nusselt number are observed for higher values of Prandtl number.

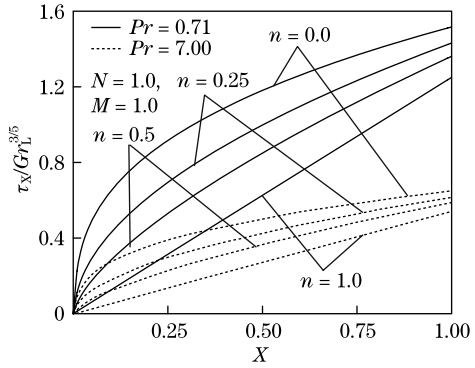

Fig. 12 Steady state local skin friction for different Pr and n

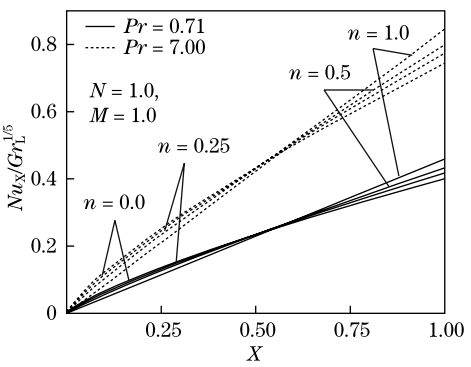

Fig. 13 Steady state local Nusselt number for different Pr and n

Transient and steady state local shearing stress and the rate of heat transfer at the leading edge of the cone for different values of magnetic field parameter M and radiation parameter N are shown in Figs. 14–17. The local wall shear stress decreases with the increasing value of M and N. The local rate of heat transfer decreases as M increases while increases as N increases since the drag force has reduced the velocity and increase the temperature.

The average skin friction and Nusselt number are presented in Figs. 18–20 for different values of Pr, n, N, and M. The influence of n on average skin friction is more when exponent n is reduced. The average wall shear stress decreases as Pr increases because velocity decreases with an increasing value of Pr as shown in Fig. 2. Also, from these figures, we remark that as the magnetic field parameter M increases the average skin friction decreases. Thus, the presence of the magnetic field helps in reducing the frictional drag on the limiting surface. Also we notice that the average wall shear stress decreases as the radiation parameter N increases because by

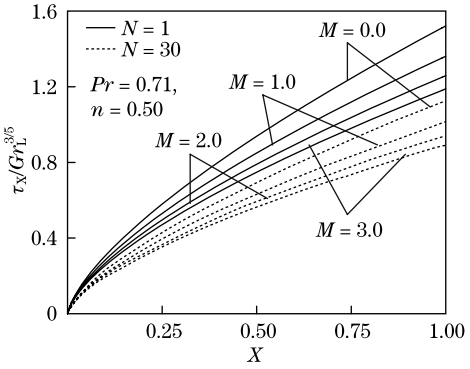

Fig. 14 Steady state local skin friction for different N and M

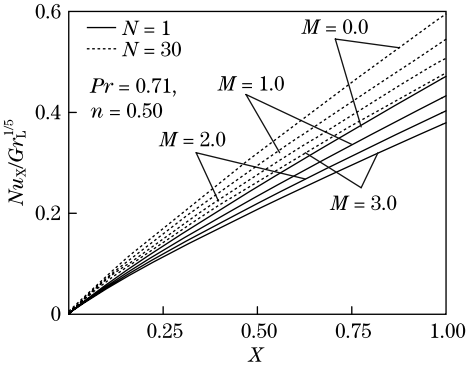

Fig. 15 Steady state local Nusselt number for different N and M

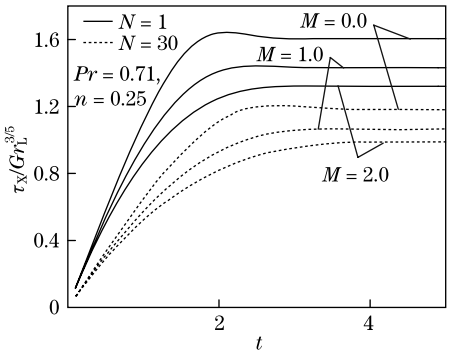

Fig. 16 Transient local skin friction at $X = 1.0$ for different N and M

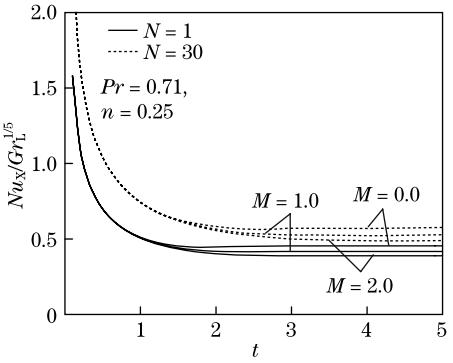

Fig. 17 Transient local Nusselt number at $X = 1.0$ for different N and M

increasing the radiation parameter N tends to reduce the velocity as shown in Fig. 6.

At initial time, higher values of average Nusselt numbers were observed. They decreased with time and become steady state after some time. It was observed that for short time, the average Nusselt number was constant at each level of various parameters. This shows that initially there is only heat conduction. Figure 19 shows that there is no significant influence of n on the average Nusselt number. The average Nusselt number became reduced by the increasing value of the magnetic field parameter M. But it also gets reduced by the decreasing value of exponent n (or) radiation parameter N. The average Nusselt number was found to decrease with the decreasing value of the Prandtl number of the fluid.

6 Concluding remarks

A mathematical model has been presented for the unsteady natural convection heat transfer from a vertical cone with combined effects of MHD and thermal radiation. The surface of the vertical cone is subjected to variable surface heat flux. The governing boundary layer equations have been non-dimensionalised and solved using the finite difference method.

(i) In the presence of magnetic field, increases of the strength of the applied magnetic field decelerates the fluid motion along the wall of the cone inside the boundary layer whereas the temperature of the fluid along the wall of the cone increases as the strength of the magnetic field increases.

(ii) The influence of exponent n and the local skin friction is observed to be large near the

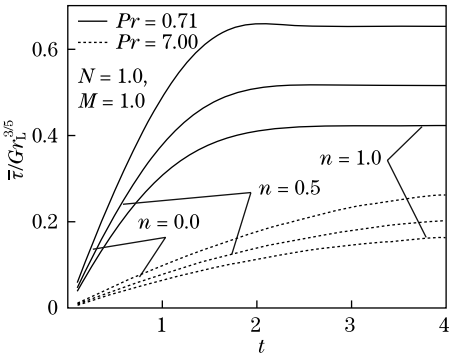

Fig. 18 Average skin friction for different Pr and n

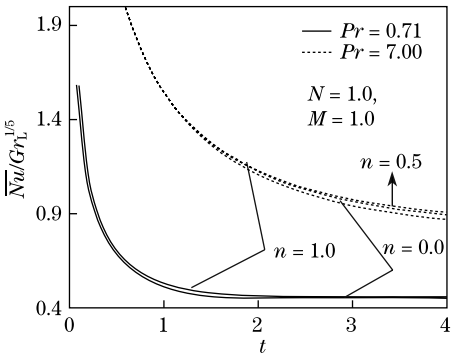

Fig. 19 Average Nusselt number for different Pr and n

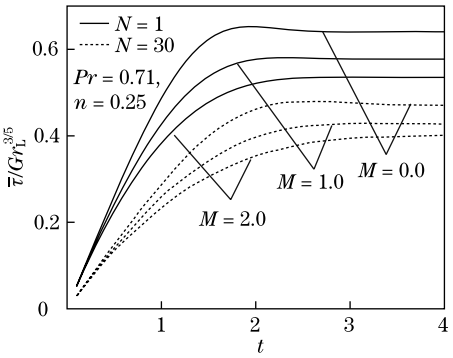

Fig. 20 Average skin friction for different N and M

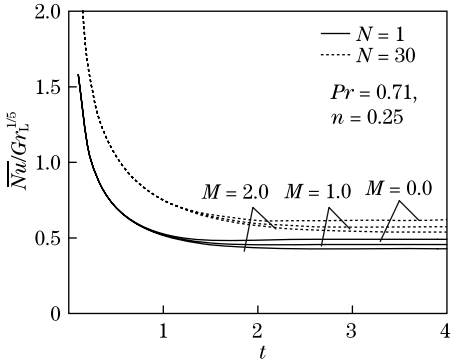

Fig. 21 Average Nusselt number for different N and M

apex of the cone, and it reduces slowly with increasing distance from the apex.

(iii) Dimensionless temperature is also seen to be decrease owing to an increase in thermal radiation.

(iv) Steady state velocity profile attains very quickly for higher values of radiation parameter N in comparison with the lower radiation parameter, which implies that the existence of radiation helps to achieve the steady state quickly.

(v) Due to the presence of radiation, the average skin friction decreases.

References

[1] Merk, H. J. and Prins, J. A. Thermal convection laminar boundary layer I. *Appl. Sci. Res.*, **4**, 11–24 (1954)

[2] Merk, H. J. and Prins, J. A. Thermal convection laminar boundary layer II. *Appl. Sci. Res.*, **4**, 195–206 (1954)

[3] Alamgir, M. Overall heat transfer from vertical cones in laminar free convection: an approximate method. *ASME Journal of Heat Transfer*, **101**, 174–176 (1989)

[4] Pop, I. and Takhar, H. S. Compressibility effects in laminar free convection from a vertical cone. *Appl. Sci. Res.*, **48**, 71–82 (1991)

[5] Pop, I., Grosan, T., and Kumar, M. Mixed convection along a vertical cone for fluids of any Prandtl number case of constant wall temperature. *International Journal of Numerical Methods for Heat Fluid Flow*, **13**, 815–829 (2003)

[6] Takhar, H. S., Chamkha, A. J., and Nath, G. Effect of thermo-physical quantities on the natural convection flow of gases over a vertical cone. *Int. J. Eng. Sci.*, **42**, 243–256 (2004)

[7] Lin, F. N. Laminar convection from a vertical cone with uniform surface heat flux. *Letters in Heat Mass Transfer*, **3**, 49–58 (1976)

[8] Na, T. Y. and Chiou, J. P. Laminar natural convection over a frustum of a cone. *Appl. Sci. Res.*, **35**, 409–421 (1979)

[9] Gorla, R. S. R., Krishnan, V., and Pop, I. Natural convection flow of a power-law fluid over a vertical frustum of a cone under uniform heat flux conditions. *Mech. Res. Comm.*, **21**, 139–146 (1994)

[10] Kumari, M. and Pop, I. Free convection over a vertical rotating cone with constant wall heat flux. *Int. J. Appl. Mech. Engg.*, **3**, 451–464 (1998)

[11] Hossain, M. A., Paul, S. C., and Mandal, A. C. Natural convection flow along a vertical circular cone with uniform surface temperature and surface heat flux in a thermally stratified medium. *International Journal of Numerical Methods for Heat Fluid Flow*, **12**, 290–305 (2002)

[12] Bapuji, P. J., Ekambavannan, K., and Pop I. Transient laminar free convection from a vertical cone with non-uniform surface heat flux. *Studia Mathematica*, **1**, 75–99 (2008)

[13] Sparrow, E. M. and Cess, R. D. The effect of a magnetic field on free convection heat transfer. *International Journal of Heat and Mass Transfer*, **3**(4), 267–274 (1961)

[14] Cess, R. D. The interaction of thermal radiation with free convection heat transfer. *International Journal of Heat and Mass Transfer*, **9**(11), 1269–1277 (1966)

[15] Kumari, M. and Nath, G. Development of two dimensional boundary layer with an applied magnetic field due to an impulsive motion. *Indian J. Pure Appl. Math.*, **30**, 695–708 (1999)

[16] Takhar, H. S., Chamkha, A. J., and Nath, G. Unsteady mixed convection flow from a rotating vertical cone with magnetic field. *Heat and Mass Transfer*, **39**, 297–304 (2003)

[17] Ozturk, A. Unsteady laminar mixed convection about a spinning sphere with a magnetic field. *Heat and Mass Transfer*, **41**, 864–874 (2005)

[18] Chamkha, A. J. and Al-Mudhaf, A. Unsteady heat and mass transfer from a rotating vertical cone with a magnetic field and heat generation or absorption effects. *Int. J. Therm. Sci.*, **44**, 267–276 (2005)

[19] Mehmet, C. E. Free convection flow about a vertical spinning cone under a magnetic field. *Applied Mathematics and Computation*, **179**, 231–242 (2006)

[20] Soundalgekar, V. M. and Takhar, H. S. Radiation effects on free convection flow past a semi-infinite vertical plate. *Modelling Measurement and Control*, **51**, 31–40 (1993)

[21] Hossain, M. A. and Takhar, H. S. Radiation effects on mixed convection along a vertical plate with uniform surface temperature. *Heat and Mass Transfer*, **31**, 243–248 (1996)

[22] Raptis, A. and Perdikis, C. Radiation and free convection flow past a moving plate. *Int. J. Appl. Mech. Eng.*, **4**(4), 817–821 (1999)

[23] Muthucumaraswamy, R. and Ganesan, P. Radiation effects on flow past an impulsively started infinite vertical plate with variable temperature. *Int. J. Appl. Mech. Eng.*, **8**(1), 125–129 (2003)

[24] Raptis, A. and Massalas, C. V. Magnetohydrodynamic flow past a plate by the presence of radiation. *Heat and Mass Transfer*, **34**, 107–109 (1998)

[25] Yih, K. A. Radiation effects on mixed convection over an isothermal cone in porous media. *Heat and Mass Transfer*, **37**, 53–57 (2001)

[26] Takhar, H. S., Beg, O. A., Chamkha, A. J., Filip, D., and Pop, I. Mixed radiation-convection boundary layer flow of an optically dense fluid along a vertical flat plate in a non-Darcy porous medium. *Int. J. Appl. Mech. Eng.*, **8**(3), 483–496 (2003)

[27] Ahmed, A. A. The effect of radiation on free convective flow and mass transfer past a vertical isothermal cone surface with chemical reaction in the presence of a transverse magnetic field. *Can. J. Physics*, **82**, 447–458 (2004)

[28] Beg, O. A., Zueco, J., Takhar, H. S., and Beg, T. A. Network numerical simulation of impulsively-started transient radiation-convection heat and mass transfer in a saturated darcy-forchheimer porous medium. *Nonlinear Analysis*: *Modelling and Control*, **13**(3), 281–303 (2008)

[29] Abd El-Naby, M. A., Elbarbary, E. M. E., and AbdElazem, N. Y. Finite difference solution of radiation effects on MHD unsteady free-convection flow over vertical porous plate. *Applied Mathematics and Computation*, **151**, 327–346 (2004)

[30] Roming, M. F. The influence of electric and magnetic fields on heat transfer to electrically conducting fluid. *Advances in Heat Transfer*, **1**, 267–354 (1964)

[31] Brewester, M. Q. *Thermal Radiative Transfer and Properties*, John Wiley and Sons, New York (1992)

[32] Carnahan, B., Luther, H. A., and Wilkes, J. O. *Applied Numerical Methods*, John Wiley and Sons, New York (1969)